# Band structure and optical properties of sinusoidal superlattices: $ZnSe_{1-x}Te_x$

G. Yang, S. Lee, and J. K. Furdyna
*Department of Physics, University of Notre Dame, Notre Dame, Indiana 46556*
(Received 14 May 1999)

This paper examines the band structure and optical selection rules in superlattices with a sinusoidal potential profile. The analysis is motivated by the recent successful fabrication of high quality $ZnSe_{1-x}Te_x$ superlattices in which the composition $x$ varies *sinusoidally* along the growth direction. Although the band alignment in the $ZnSe_{1-x}Te_x$ sinusoidal superlattices is staggered (type II), they exhibit unexpectedly strong photoluminescence, thus suggesting interesting optical behavior. The band structure of such sinusoidal superlattices is formulated in terms of the nearly-free-electron (NFE) approximation, in which the superlattice potential is treated as a perturbation. The resulting band structure is unique, characterized by a single minigap separating two wide, free-electron-like subbands for both electrons and holes. Interband selection rules are derived for optical transitions involving conduction and valence-band states at the superlattice Brillouin-zone center, and at the zone edge. A number of transitions are predicted due to wave-function mixing of different subband states. It should be noted that the zone-center and zone-edge transitions are especially easy to distinguish in these superlattices because of the large width of the respective subbands. The results of the NFE approximation are shown to hold surprisingly well over a wide range of parameters, particularly when the period of the superlattice is short.

## I. INTRODUCTION

Semiconductor superlattice structures have been receiving a great deal of attention for the last few decades due to their attractive electronic and optical properties. Most studies, however, are carried out on superlattices in the form of a succession of square wells, resulting from *abrupt* interfaces betwen constituent layers. Only a few references exist in the literatures to compositionally modulated superlattices,[1,2] because fabrication of such superlattices is difficult (or even unrealistic) with normal molecular-beam-epitaxy (MBE) growth techniques. It was recently reported[3] that $ZnSe_{1-x}Te_x$ superlattices (SL's) can be grown by molecular-beam epitaxy with a composition profile that varies *sinusoidally* along the growth direction. Such sinusoidal modulation of the composition $x$ is expected to lead to interesting physical properties in these structures. For example, in our optical studies of these structures we have already noted that—although the above SL's have a type-II band alignment—they show unexpectedly intense photoluminescience.[4]

Because of these special features, it is interesting to ask how the band structure of these SL's differs from that of conventional SL's, grown as a succession of square-well potentials. Our objective, then, is to formulate the electronic band structure of sinusoidal SL's, with special attention paid to optical transitions which result from such a band structure. It turns out that SL's with a sinusoidal potential profile are especially amenable to an analytical description in terms of the nearly-free-electron (NFE) approximation. Using this model, we will derive analytic expressions for the energies, the wave functions, and the effective masses at the minigaps of such SL's. We will then use these results to discuss the optical properties of the structures. As will be seen, a number of optical transitions will emerge due to the wave-function mixing of different subbands. It will be shown, furthermore, that in systems of this type transitions which occur at the Brillouin-zone center can be readily distinguished from those occurring at the zone edges.

## II. BAND STRUCTURE OF SUPERLATTICES WITH SINUSOIDAL ENERGY PROFILES

We begin by considering a single band of a sinusoidally modulated SL. For specificity, we will expicitly discuss the conduction band, as schematically shown in Fig. 1. The behavior of an electron in the conduction band is determined by the standard Schrödinger equation

$$H\Psi(z)=\left[-\frac{\hbar^2}{2m^*}\frac{d^2}{dz^2}+V(z)\right]\Psi(z)=E\Psi(z), \qquad (1)$$

where $H$ is the Hamiltonian, $m^*$ is the effective mass, and $E$ represents the eigenenergies of the system. In the case of a sinusoidal SL, the potential $V(z)$ is given by

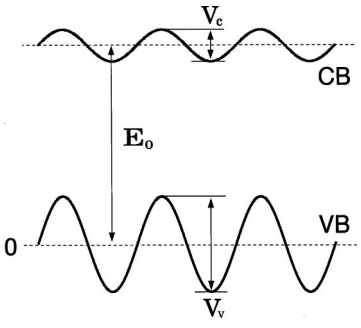


FIG. 1. Energy-band profile of a sinusoidal superlattice for the conduction and valence bands with a type-II alignment. The valence-band offset is assumed to be larger, to qualitatively simulate the specific case of $ZnSe_{1-x}Te_x$ superlattices considered in this paper.

 

$$V(z)=\frac{1}{2}V\cos\left(\frac{2\pi z}{L}\right), \tag{2}$$

where $L$ is the SL period, $z$ is the SL growth direction, and $V$ is the peak-to-peak value of the band offset of the band under consideration. The potential $V(z)$ can be expanded as a Fourier series, with the Fourier coefficients $V_n$ of the series given by

$$V_n=\frac{1}{4}V\delta_{n,1}; \tag{3}$$

i.e., all Fourier components of $V(z)$ vanish except $V_1$. This feature, specific to the sinusoidal profile, results in a major simplification of the band structure.

In the NFE approximation, it is assumed that $V(z)$ is small in comparison with kinetic-energy terms in Eq. (1). We can thus treat $V(z)$ as a perturbation. Since in sinusoidal SL's only $V_1\neq 0$, it is readily shown that, to first order, only one minigap opens: the first minigap at $k=\pm\pi/L$,[5,6] with the minigap width given by

$$E_{g,1}=2|V_1|=\frac{1}{2}V. \tag{4}$$

It is interesting to note that this minigap is determined *only* by the value of the band offset. Such a characteristic band structure is shown schematically in Fig. 2 in extended zone form. The wave functions associated with the two energy extrema of this minigap are $\cos(n\pi z/L)$ and $\sin(n\pi z/L)$, their order (which one is upper, and which is lower) depending on the sign of $V_1$.[5,7]

The effective masses associated with such a minigap are given by the very convenient analytic expressions derived in Appendix B of Ref. 6,

$$m^*_{1+}=-m^*_{1-}=\frac{m^*E_{g,1}}{4T_1}, \tag{5}$$

where the $+$ and $-$ subscripts refer to the higher- and lower-lying states, and $T_1$ is the kinetic-energy term at the zone edge, defined as

$$T_1=\frac{\hbar^2\pi^2}{2m^*L^2}.$$

To second order, the minigap at $k=\pm 2\pi/L$ will also open. With the Fourier coefficients given by Eq. (3), we obtain the minigap widths, wave functions, and effective masses at the $k=\pm 2\pi/L$ minigap (see the Appendixes of Ref. 6):

$$E_{g,2}=\frac{V^2}{8T_2}, \qquad m^*_2=\frac{m^*V^2}{32T_2}. \tag{6}$$

It is noted that the magnitudes of $E_{g,2}$ and $m^*_2$ are indeed much smaller than $E_{g,1}$ and $m^*_1$. The wave functions for the two extrema associated with this minigap are $\cos(2\pi z/L)$ and $\sin(2\pi z/L)$, respectively. A detailed analysis shows that a third-order perturbation analysis is required for the third minigap to open; the fourth minigap will open in fourth order, and so on. It is thus a characteristic of sinusoidal SL's

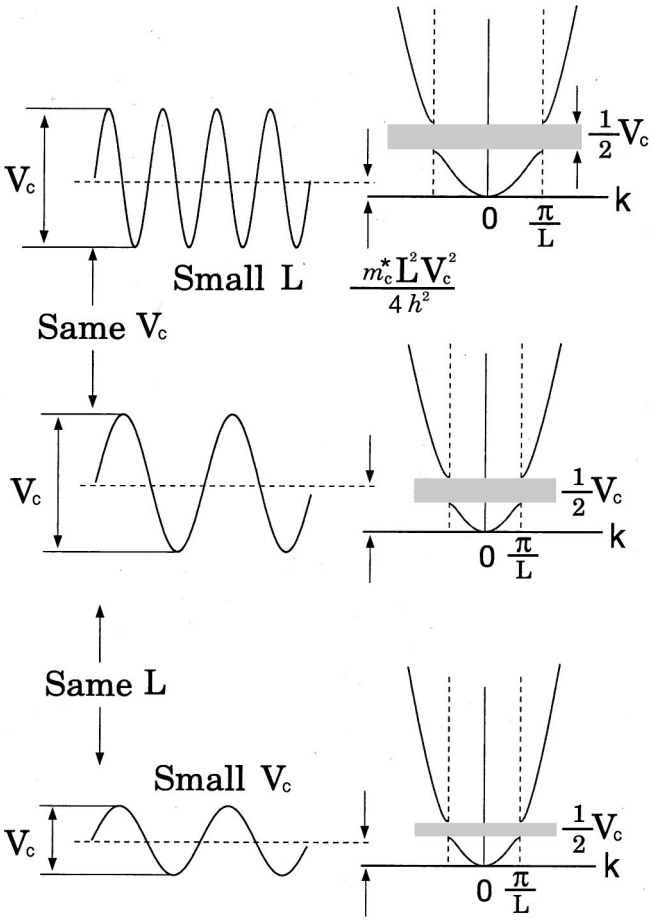


FIG. 2. Band structure of superlattices with sinusoidal energy profile. Only a single band gap appears at the zone edge in first-order perturbation analysis. Note the shift of the band edge below the compositional average by the amount $m^*_cL^2V_c^2/4h^2$ [according to Eq. (7)].

that, as perturbation theory is carried to higher orders, each additional order $n$ reveals a new minigap at the successive values of $k=n\pi/L$. But the widths of these minigaps (and the corresponding densities of states at the extrema) decrease extremely rapidly with $n$, as does their physical importance. Wave functions for several lower-order minigaps in the conduction band are listed in Table I.

Using first- and second-order perturbation analyses, we can obtain the energy shift of the band edge for both the conduction and valence bands. At the $\Gamma$ point ($q=0$),

$$E(e1_0)=E_0-\frac{2V_{1c}^2}{T_{2c}}, \qquad E(\mathrm{hh}1_0)=\frac{2V_{1v}^2}{T_{2v}}, \tag{7}$$

$$E(\mathrm{hh}3_0)=-T_{2v}-\frac{V_{1v}^2}{T_{2v}}. \tag{8}$$

Here we denote specific subband states by $eN_q$ and $\mathrm{hh}N_q$, where $e$ and hh stand for ''electron'' and ''heavy hole,'' $N$ is the subband index (starting from that closest to the bottom of the well for conduction electrons, and from the top of the well for the holes), and $q$ is the SL wave vector. In our notation $q=0$ and 1 represent the superlattice Brillouin-zone center and zone edge (i.e., $q=\pi/L$), while $k$ is used to de-

TABLE I. Wave functions for several lowest conduction subband states, showing admixtures from the nearest-neighboring states. The admixture parameters an $\delta_c = V^c/(\pi T_2^c)$ and $\delta_v = V^v/(\pi T_2^v)$.

| State | Wave function |
|---|---|
| $e1_0$ | $1+2\delta_c\cos\left(\frac{2\pi z}{L}\right)$ |
| $e1_1$ | $\cos\left(\frac{\pi z}{L}\right)+\frac{1}{2}\delta_c\cos\left(\frac{3\pi z}{L}\right)$ |
| $e2_1$ | $\sin\left(\frac{\pi z}{L}\right)-\frac{1}{2}\delta_c\sin\left(\frac{3\pi z}{L}\right)$ |
| $e2_0$ | $\sin\left(\frac{2\pi z}{L}\right)-\frac{2}{9}\delta_c\sin\left(\frac{4\pi z}{L}\right)$ |
| $e3_0$ | $\cos\left(\frac{2\pi z}{L}\right)-\delta_c+\frac{4}{9}\delta_c\cos\left(\frac{4\pi z}{L}\right)$ |
| $e3_1$ | $\sin\left(\frac{3\pi z}{L}\right)+\frac{1}{2}\delta_c\sin\left(\frac{\pi z}{L}\right)-\frac{1}{4}\delta_c\sin\left(\frac{5\pi z}{L}\right)$ |
| $e4_1$ | $\cos\left(\frac{3\pi z}{L}\right)-\frac{1}{2}\delta_c\cos\left(\frac{\pi z}{L}\right)+\frac{1}{4}\delta_c\cos\left(\frac{5\pi z}{L}\right)$ |

note points in the Brillouin zone in the bulk material. To define a point of reference for the energy, we have taken the center of the valence band (midpoint between extrema) as the zero point, as shown by the lower dotted line in Fig. 1; $E_0$ is the energy separation from the center of the valence band to the center of the conduction band (see Fig. 1); and

$$T_{nc,v}=\frac{\hbar^2\pi^2n^2}{2m^*_{c,v}L^2}, \qquad V_{1c,v}=\frac{1}{4}V_{c,v}, \tag{9}$$

where $V_{c,v}$ are the peak-to-peak offset values for the conduction and valence bands, respectively. Thus, according to Eq. (7), the lowest electron energy level of $E(e1)$ is slightly below the center of the conduction band (pushed down by an amount $2V_{1c}^2/T_{2c}$), and the ground-state heavy-hole energy $E(\mathrm{hh1})$ is slightly above the center of the valence band (pushed up by the amount $2V_{1v}^2/T_{2v}$). For $E(\mathrm{hh3})$, the kinetic-energy term has a minus sign because the dispersion curvature for holes is downward. Several examples of transition energies allowed at the $\Gamma$ point are

$$\mathrm{hh1}_0\rightarrow e1_0: \qquad E_0-2\left(\frac{V_{1c}^2}{T_{2c}}+\frac{V_{1v}^2}{T_{2v}}\right), \tag{10}$$

$$\mathrm{hh3}_0\rightarrow e1_0: \qquad E_0+T_{2v}+\left(\frac{V_{1v}^2}{T_{2v}}-\frac{2V_{1c}^2}{T_{2c}}\right). \tag{11}$$

Similarly, energies of band extrema at the superlattice zone edge $(q=1)$ are

$$E(e1_1)=E_0+T_{1c}-V_{1c}, \qquad E(e2_1)=E_0+T_{1c}+V_{1c}, \tag{12}$$

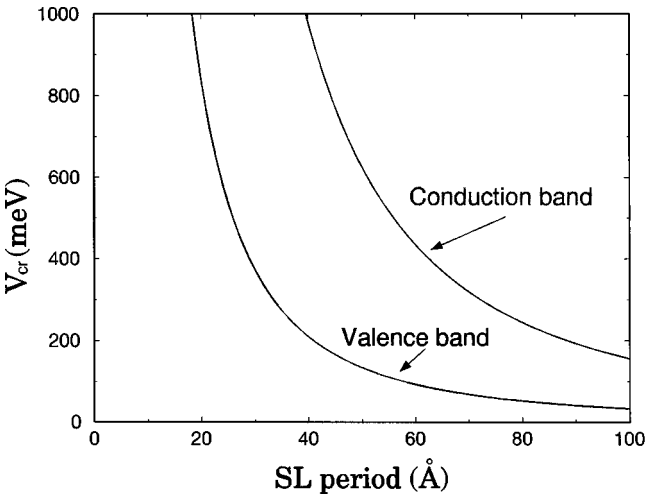


FIG. 3. Relationship between the critical band offset $V_{cr}$ and the superlattice period obtained from the NFE model in sinusoidal SL. The NFE approximation holds for values of $L$ to the left of the curves for each band, respectively.

$$E(\mathrm{hh1}_1)=-T_{1v}+V_{1v}, \qquad E(\mathrm{hh2}_1)=-T_{1v}-V_{1v}. \tag{13}$$

Examples of transition energies allowed at the $q=1$ point are then given by

$$\mathrm{hh1}_1\rightarrow e2_1: \qquad E_0+(T_{1c}+T_{1v})-(V_{1v}-V_{1c}), \tag{14}$$

$$\mathrm{hh2}_1\rightarrow e1_1: \qquad E_0+(T_{1c}+T_{1v})+(V_{1v}-V_{1c}). \tag{15}$$

These transitions will be discussed in more detail in Secs. III and IV, later in the paper.

The criterion for the applicability of the NFE approximation was given in Ref. 6. The NFE can be applied with confidence as long as the offset is lower than the value

$$V=\frac{\hbar^2\pi^3}{m^*}\frac{1}{L^2}. \tag{16}$$

It can be seen from this condition that the shorter the SL *period*, the higher can be the actual value of the offset $V$ satisfying the perturbation condition. We illustrate these features in Fig. 3, which shows the estimates of the upper limit of $V$ for both the conduction- and valence-band offsets obtained from Eq. (16), for the perturbation theory to be applicable. In these estimates we have assumed that the electron effective mass is $0.15m_0$ (typical for ZnSe and other wide-gap II-VI semiconductors), and that the heavy-hole mass is five times larger than the electron effective mass—a situation characteristic of many wide-gap semiconductor compounds.[8] It can be seen from Fig. 3 that the condition for the applicability of the perturbation theory rapidly relaxes as the period of the SL becomes smaller.

## III. PHOTOLUMINESCENCE IN $ZnSe_{1-x}Te_X$ SYSTEMS

The $ZnSe_{1-x}Te_x$ superlattices studied experimentally in this paper were fabricated by means of a MBE growth technique, in which the periodic modulation is achieved by substrate rotation in the presence of nonuniform flux distributions of Se and Te, rather than shutter openings and closings.

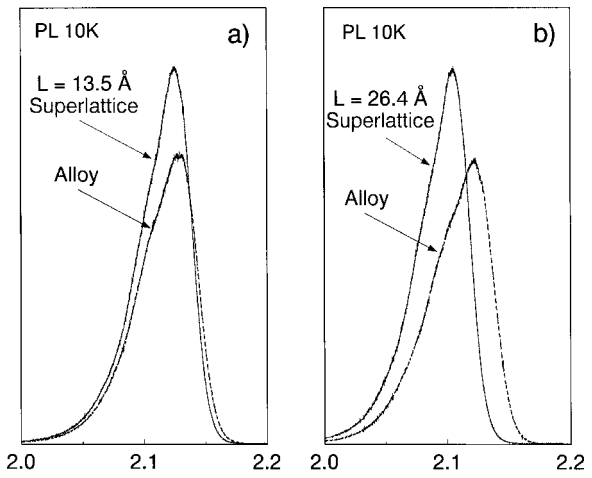


FIG. 4. PL spectra for $ZnSe_{1-x}Te_x$ alloy and for $ZnSe_{1-x}Te_x$ SL's with sinusoidal modulation. Panels (a) and (b) are for SL's with 13.5- and 26.4-Å periods, respectively.

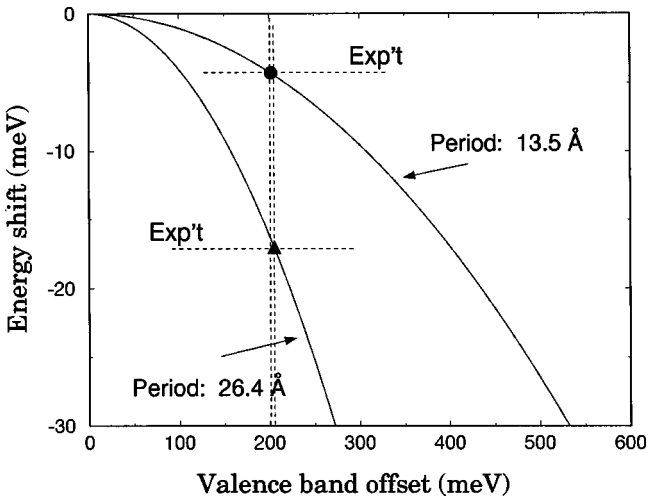


FIG. 5. Energy shifts of band-edge transitions as functions of the valence-band offset, calculated for SL's with 13.5- and 26.4-Å periods, as discussed in the text (solid curves). Experimental shifts of the PL peak observed for the two SL's relative to the corresponding alloy are shown as horizontal dotted lines. The intersection of the dotted line and the calculated (solid) curve gives an estimate of the valence-band offset for the two SL's (both very close to 200 meV).

With this technique, we were able to grow massive superlattices, of multimicron thicknesses and with many hundreds of periods. Due to such massive structure, one can ignore the strain caused by the lattice mismatch between the substrate and superlattice, even though the superlattices are grown on GaAs substrates. That is, after the structure exceeds a critical thickness (in the first few hundred nanometers), it becomes free standing. We thus do not include the effects of strain in the analysis of the optical results obtained on these superlattices. For further details about the growth procedure, the reader is referred to Ref. 9.

We examined the optical properties of sinusoidal SL's using the band structure formulated in Sec. II. We first consider transitions associated with the band edge (i.e., the $\Gamma$ point), because these are expected to dominate the optical spectrum. To illustrate the analysis, we will use $ZnSe_{1-x}Te_x$ sinusoidal SL's with two different periods, but with the same modulation amplitude of $x$, as determined by x-ray studies ($x$ varies from 0.35 to 0.65).[9]

In this specific $ZnSe_{1-x}Te_x$ system, the largest band-gap difference between the two layers (i.e., the band-gap difference between $ZnSe_{0.65}Te_{0.35}$ and $ZnSe_{0.35}Te_{0.65}$) is about 130 meV.[10] Since the band alignment is known to be of type II in this system (as shown in Fig. 1), the valence-band offset is expected to be larger than the 130-meV band-gap difference. Thus the band offsets are themselves not small. However, in the case of very short period SL's the NFE approximation can be applied even for moderately large band offsets, as seen in Fig. 3. In the SL's under consideration, the periods are 13.5 and 26.4 Å, as determined by x-ray measurements.[9] As shown in Fig. 3, these short periods extend the validity of the NFE approximation to the values of $V^v \approx 400$ meV and $V^c \approx 1000$ meV. Both the valence- and conduction-band offsets in these systems are not expected to exceed the above limits, and the NFE approximation can thus be applied to these systems.[11]

The photoluminescence (PL) spectra for the two $ZnSe_{1-x}Te_x$ sinusoidal SL's are shown in Fig. 4. The results obtained on the two superlattices (periods $L = 13.5$ and 26.4 Å) have been separated into two panels for clarity. In each panel, there are two spectra, one taken on a sinusoidal SL, and one on the alloy $ZnSe_{1-x}Te_x$ whose composition is the same as the average composition of the SL. It is clear that the redshift of the superlattice PL position relative to the corresponding alloy is much larger in the case of the SL with the longer period. This behavior of the PL energy is exactly as anticipated by the band-edge shift [see Eqs. (7) and (10)] obtained in the NFE model presented above.

For a quantitative analysis of this result, we can rewrite the transition energies at the $\Gamma$ point by re-expressing $V_1$ and $T_2$ in Eq. (10) explicitly in terms of $V, L$, and $m^*$:

$$\mathrm{hh}1_0 \rightarrow e1_0: \qquad E_0 - \frac{L^2}{16\hbar^2\pi^2}(V_c^2 m_c^* + V_v^2 m_v^*). \quad (17)$$

The energy shift is now a function of the carrier effective masses, the band offsets in both bands, and the SL period. We note immediately that, as a good approximation, we can ignore the contribution from the conduction band in Eq. (17), since the electron mass is five times smaller, and the band offset is at least two times smaller, than the corresponding quantities in the heavy-hole band. Thus the redshift from $E_0$ is almost entirely dominated by the valence-band parameters.

Figure 5 shows the plots (solid curves) of the energy shifts as a function of the valence band offset for sinusoidal SL's with 13.5-and 26.4 Å periods obtained using the value of $0.7m_0$ for the heavy-hole mass. These energy shifts between the average alloy ($V=0$) and the SL can then be used to find the valence-band offset in each sinusoidal SL. We draw the energy shifts observed experimentally for the 13.5- and 26.4-Å SLs (4 and 17 meV, respectively; see Fig. 4) as horizontal dotted lines in Fig. 5. The crossing points of these lines with the corresponding calculated curves then give a very close estimate of the valence-band offset. The values obtained in this way are $V=202$ meV for the SL with the 13.5-Å period, and $V=205$ meV for the 26.4-Å SL. Recall-

ing that the two SL's have identical compositional modulation amplitudes, it is very gratifying that the value of the valence-band offsets obtained from the two specimens, 202 and 205, are very close to one another (as indeed they should be). This value for the valence-band offset automatically gives the conduction-band offset to be about 70 meV, since the maximum band-gap difference for this modulation ($0.35<x<0.65$) is 130 meV. The band offsets for both bands turn out to be very small compared to the critical values plotted in Fig. 3, as had been assumed *a priori* in our analysis of the PL data.

## IV. SELECTION RULES FOR OPTICAL TRANSITIONS

The above successful description of the fundamental PL data encourages us to consider other optical transitions in sinusoidal $ZnSe_{1-x}Te_x$ SL's. We will restrict ourselves to transitions between the conduction band and the *heavy-hole* valence band, because these transitions dominate the interband optical spectra. For traditional large-offset staggered (type-II) superlattices, the parity selection rules cannot be applied, because the electrons and holes are separated in space. It has been shown, however, that for type-II superlattices which satisfy the small band-offset condition, rigorous selection rules can be found, similar to those in type-I structures.[6,12] In fact, there is no qualitative distinction between type-I and -II configurations as long as Eq. (16) is satisfied.

To obtain the selection rules for optical transitions, we need to evaluate the wave function overlaps $\langle\psi_i|\psi_f\rangle$, where $\psi_i$ and $\psi_f$ are the wave functions associated with the initial and the final states, respectively. When the offset is very small, the $\sin(n\pi z/L)$ and $\cos(n\pi z/L)$ functions obtained from first-order perturbation analysis provide a good description of the wave functions of the states at the $n$th gap. However, it has been shown that—as the offset increases [although still satisfying the ''smallness'' criterion given by Eq. (16) and Fig. 3]—it will progressively bring about admixtures from other nearby subband states into the wave function under consideration.[5,6] The band structure and second-order wave functions at $q=0$ and 1 for sinusoidal SL's are shown in Fig. 6. Only admixtures from the nearest-neighboring subbands to the first-order wave functions are included. The admixture parameter $\delta_c(\delta_v)$ is defined as $V^c/\pi T_2^c\,(V^v/\pi T_2^v)$, where the superscript $c(v)$ stands for conduction band (valence band), $V$ is the band offset, and $T_2$ is the kinetic energy. It should be noted that in Fig. 6 we only show the wave functions for minigaps up to $n=2$. The minigap at $k=\pm n\pi/L$ for $n\geqslant 3$ remain closed even to second-order perturbation. As a result, the densities of states associated with these higher minigaps are extremely small, and optical transitions occurring at these points are expected to be correspondingly very weak. We can then ignore these minigaps when discussing optical transitions of sinusoidal SLs.

The optical transition intensity is determined by the wave-function overlap of the initial and the final state, together with the joint density of states associated with the transition. Table II lists the wave-function overlap within one SL period for a series of transitions, calculated using the NFE model for a sinusoidal SL with a period of 30 Å. The table also gives the calculated reduced masses $\mu_z$ corresponding to these transitions, which can be used as a measure of the joint density of states according to Eq. (37) in Ref. 6. The intensities of the transitions ($I_{i\to j}$) were estimated from the product of the square of the wave-function overlap and the square root of $\mu_z$. These estimated intensities (normalized to the $hh1_0\to e1_0$ transition) are also shown in Table II, except for those cases where $\mu_z<0$. A negative $\mu_z$ is associated with a so-called $M_1$ saddle point, and intensities of transitions involving such a saddle point are expected to be vanishingly weak.[13,14]

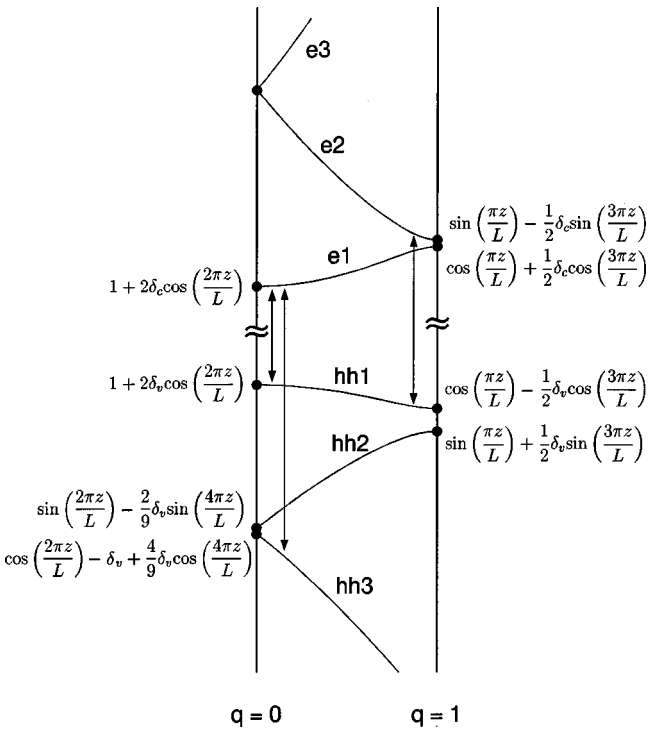


FIG. 6. Band-structure and corresponding wave functions, up to second-order perturbation analysis. Strongest transitions (as predicted in Table II) are shown by arrows.

We begin by considering transitions at the SL Brillouin-zone center. From Table II, one can see that the $hh1_0\to e1_0$ transition is the strongest, primarily due to the highest joint density of states. The effective mass is much smaller at

TABLE II. Reduced masses, wave-function overlaps, and transition intensities for various transitions calculated for a $ZnSe_{1-x}Te_x$ sinusoidal SL with a period $L$ of 30 Å.

| Transition | $\mu_z$ | $\langle\psi_i\|\psi_j\rangle$ | $I_{i\to j}$ |
|---|---|---|---|
| $hh1_0\to e1_0$ | $+0.29$ | 0.90 | 1.0 |
| $hh2_0\to e2_0$ | $-0.58\times10^{-4}$ | 0.96 | $\mu_z<0$ |
| $hh3_0\to e3_0$ | $+0.58\times10^{-4}$ | 0.88 | 0.016 |
| $hh3_0\to e1_0$ | $+0.0243$ | 0.59 | 0.125 |
| $hh1_0\to e3_0$ | $+0.58\times10^{-4}$ | 0.59 | 0.06 |
| $hh1_1\to e2_1$ | $+0.797\times10^{-2}$ | 0.98 | 0.19 |
| $hh2_1\to e1_1$ | $-0.85\times10^{-2}$ | 0.93 | $\mu_z<0$ |

[a]The intensity is normalized to 1.0 for the $hh1_0\to e1_0$ transition.

the $n=2$ minigap, which is closed in first order [see Eq. (6)]. Thus the $hh2_0 \rightarrow e2_0$ and $hh3_0 \rightarrow e3_0$ transitions should be very weak (in spite of the fact that they are both $\Delta N=0$ transitions), due to the much smaller joint density of states associated with the extremely small minigap for $n=2$ at the zone center (see Fig. 6). For this reason we expect all transitions involving states $e2_0$ and $e3_0$ to be negligible.

As can be seen from Table II, the NFE model predicts the $hh3_0 \rightarrow e1_0$ transition to be the second strongest transition at $q=0$. This is a $\Delta N \neq 0$ transition, which becomes allowed due to wave-function mixing. This transition serves very nicely to illustrate the role of joint density of states in determining transition intensity: the ''forbidden'' $hh3_0 \rightarrow e1_0(\Delta N=2)$ transition is much stronger than the ''allowed'' $hh3_0 \rightarrow e3_0(\Delta N=0)$ transition, because the density of states associated with the $e1_0$ subband is much higher than that for $e3_0$. Another expected $\Delta N \neq 0$ transition at $q=0$ is the $hh1_0 \rightarrow e3_0$. But the intensity of this transition is much weaker than that of $hh3_0 \rightarrow e1_0$, again because of the small density of states of the $e3_0$ state.

Next we discuss the transitions at the SL Brillouin-zone edge ($q=1$). In a type-II SL the layers which act as wells for conduction electrons constitute barriers for the holes. As a result, the ordering of $\sin(\pi z/L)$ and $\cos(\pi z/L)$ states at the $n=1$ minigap is opposite for the conduction and valence bands.[6] We thus expect the $hh1_1 \rightarrow e2_1$ and $hh2_1 \rightarrow e1_1$ transitions to be allowed. Indeed, as we note in Table II, the $hh1_1 \rightarrow e2_1$ transition has the highest wave function overlap of all (including $hh1_0 \rightarrow e1_0$). The intensity of this transition is predicted to be about one-fifth of the main transition $hh1_0 \rightarrow e1_0$. The intensity of the $hh2_1 \rightarrow e1_1$ transition, on the other hand, is expected be much weaker than that of $hh1_1 \rightarrow e2_1$, because $hh2_1 \rightarrow e1_1$ is a *saddle-point* excitonic transition (negative $\mu_z$, see Table II), as discussed in Ref. 6.

## V. SUMMARY AND CONCLUSIONS

We have examined the band structure and optical selection rules in superlattices with a *sinusoidal* potential profile. This work was motivated by the recent success in fabricating $ZnSe_{1-x}Te_x$ superlattices using a MBE growth mode that exploits the rotation of the substrate in the presence of an inhomogeneous distribution of elemental fluxes instead of shutter openings and closings.[9] The band structure of such sinusoidal superlattices was formulated in terms of the nearly-free-electron approximation, in which the superlattice potential was treated as a perturbation. The analysis results in a dispersion characterized by a single minigap separating two wide, nearly free-electron-like subbands in both the conduction and valence bands. Based on these results, we have derived selection rules for interband transitions between valence- and conduction-band states at the superlattice Brillouin-zone center and at the zone edge. A number of transitions, forbidden by the $\Delta n=0$ rule, are predicted due to wave function mixing of different subband states. It is especially interesting that the analysis allows us to conveniently distinguish between zone-center and zone-edge transitions in these structures, particularly in the case of short-period superlattices where the $q=0$ and 1 transitions have a significant energy separation due to the correspondingly large subband widths that characterize such structures.

We have used the analytic formulation presented in this paper to analyze the PL signal observed experimentally on the $ZnSe_{1-x}Te_x$ already referred to. In this connection two features are worthy of note. First, the position of the PL showed the predicted dependence on the period of the SL. Second, the intense signal observed in this system (initially rather surprising, because the band alignment of $ZnSe_{1-x}Te_x$ superlattices is expected to be staggered, or type II) could also be explained by the model, which indicates that for short-period SLs the spatial separation of electrons and holes ceases to play a major role, and fundamental ground-state transitions become direct. Our model also allowed us to obtain the value of the band offset from the PL data by analyzing data from superlattices with the same compositional modulation but different periods.

We must note finally that in the specific case of $ZnSe_{1-x}Te_x$ superlattices discussed in the experimental part of this paper, a sinusoidally modulated composition does not of itself guarantee perfect sinusoidal profile of the band edges, because of the very strong bowing of the energy gap in this material.[10] The rather good self-consistency of the band-offset results suggest, however, that the departure is not serious, and that the model provides a reasonable approximation as long as the periodic modulation is relatively smooth. We are currently exploring the effects of other than sinusoidal band-edge profiles on the superlattice band structure; and we are simultaneously exploring the fabrication of superlattices with different smooth profiles, that can be obtained by programming the speed of rotation *during each cycle* of the rotating mounting block. Once this is under control, by this shutterless technique we will be able to produce superlattices with smoothly varying periods of arbitrary shape.

## ACKNOWLEDGMENTS

We would like to express our thanks to Dr. M. Dobrowolska for valuable discussions, and to U. Bindley for her assistance in specimen fabrication. The research was supported by DOE Grant No. 97ER45644.

[1] T. Mattila, L. Bellaiche, L.-W. Wang, and A. Zunger, Appl. Phys. Lett. **72**, 2144 (1998).

[2] Y. Zhang and A. Mascarenhas, Phys. Rev. B **57**, 12 245 (1998).

[3] S.P. Ahrenkiel, S.H. Xin, P.M. Reimer, J.J. Berry, H. Luo, S. Short, M. Bode, M. Al-Jassim, J.R. Buschert, and J.K. Furdyna, Phys. Rev. Lett. **75**, 1586 (1995).

[4] S. Lee, C. S. Kim, and J. K. Furdyna (unpublished).

[5] L. A. Lewandowski, Ph.D. dissertation, University of Notre Dame, 1995.

[6] G. Yang, L.A. Lewandowski, and J.K. Furdyna, Acta Phys. Pol. A **93**, 567 (1998).

[7] J. Fang and D. Lu, *Solid State Physics* (Science and Technology, Shanghai, 1980), p. 209.

[8] *Metals. Electonic Transport Phenomena*, edited by O. Madelung,

Landolt-Börnstein, New Series, Group III, Vol. 15 (Springer, Berlin 1982).
[9] P. M. Reimer, J. R. Buschert, S. Lee, and J. K. Furdyna, Phys. Rev. B **61**, 8388 (2000).
[10] M.J.S.P. Brasil, R.E. Nahory, F.S. Turco-Sandroff, H.L. Gilchrist, and R.J. Martin, Appl. Phys. Lett. **58**, 2509 (1991).
[11] N. Dai, Ph.D. dissertation, University of Notre Dame, 1993.
[12] N. Dai, L.R. Ram-Mohan, H. Luo, G.L. Yang, F.C. Zhang, M. Dobrowolska, and J.K. Furdyna, Phys. Rev. B **50**, 18 153 (1994).
[13] H. Chu and Y.-C. Chang, Phys. Rev. B **36**, 2946 (1987).
[14] B. Deveaud, A. Chomette, F. Clerot, A. Regreny, J.C. Mann, R. Romestain, G. Bastard, H. Chu, and Y.-C. Chang, Phys. Rev. B **40**, 5802 (1989).